



Spectroscopic study of the role of alkaline earth oxides in mixed borate glasses - site basicity, polarizability and glass structure

Hosam Othman^{a,*}, Hagar Elkholy^{a,b}, Maria Rita Cicconi^{b,c}, Dimitrios Palles^d,
Dominique de Ligny^b, Efstratios I. Kamitsos^d, Doris Möncke^{d,e}

^a Physics Department, Faculty of Science, Menoufia University, Egypt

^b Department of Materials Science and Engineering, Institute of Glass and Ceramics, University of Erlangen-Nürnberg, Germany

^c Institut de Physique du Globe de Paris, 1, rue Jussieu F-75005 Paris Cedex 05, France

^d Theoretical and Physical Chemistry Institute, National Hellenic Research Foundation, Athens, Greece

^e Inamori School of Engineering at the New York State College of Ceramics, Alfred University, Alfred, NY, USA



ARTICLE INFO

Keywords:

Borate glasses
Force constant
Raman and IR spectroscopy
Structure property correlation
Optical basicity

ABSTRACT

The effect of alkaline earth ions on the structure and properties of borate glasses near the metaborate composition was studied for two glass series, 30MO-10Li₂O-10Al₂O₃-50B₂O₃ with M = Mg, Ca, Sr or Ba and xMgO-(30-x)BaO-10Li₂O-10Al₂O₃-50B₂O₃ series, for undoped and doped (0.5 mol% MnO or CuO) glasses. Thermal and optical properties, including the optical basicity, were correlated with structural variations. IR and Raman spectra showed the highest N₄ fraction for the high basicity glasses, decreasing for higher field strength ions (Ba > Sr > Ca > Mg). As determined from far IR bands the mixing of dissimilar cations affects M-O interactions. The glass transition temperature T_g correlates well to the average bond strength of the compared alkaline earth ions. The redox ratio of Mn²⁺/Mn³⁺ or Cu²⁺/Cu⁺ shifted to lower valences in low basicity glasses. The optical basicity probe ion Mn²⁺ gives consistently higher values compared to the average optical basicity, suggesting that Mn²⁺ ions seek out high basicity ligands.

1. Introduction

Borate glasses show an exceptional high solubility for rare earth or heavy metal ions, transition metal, alkali, and alkaline earth ions [1–9]. Together with their high capability to form glasses with other network formers, such as silicates and phosphates, a wide range of applications is based on borate-containing glasses including, but not being limited to, nuclear waste disposal, nonlinear or fiber optics, electronic displays or bioactive glasses [3,7,8]. In the current study, manganese and copper ions were added to the glasses as structural probe ions and for their optical properties. Dissolved copper ions are found in glasses as colorless Cu⁺ (d¹⁰) and the divalent Cu²⁺ (d⁹), which impart a blue color [9,10]. Manganese ions are usually found as nearly colorless Mn²⁺ (d⁵, double forbidden transition) and intense purple Mn³⁺ (d⁴) [9,11,12]. Mn²⁺, just as Pb²⁺, can be utilized as a probe ion for the optical basicity [13–16].

Borate glasses are characterized by extrema in the composition dependence of many glass properties, the so called “boron oxide anomaly”, and do not show the same continuous change in properties with modifier oxide addition and subsequent depolymerization of the glass network; a trend known for silicate and phosphate glasses

[7,17–20]. The boron oxide anomaly can be explained by the initial coordination change of boron from threefold in neutral B O_3^0 trigonal units to charged tetrahedral [B O_4^-] units (O denotes bridging oxygen atoms), a process increasing the network connectivity. Further addition of modifier oxides results in additional network modification, and three-fold coordinated borate units are formed with 1, 2 and, finally, 3 non-bridging oxygen atoms [2,15,20]. At high modifier oxide contents, the number of tetrahedral borate units decrease as more trigonal entities with 2 or 3 non-bridging oxygen atoms are formed. The change in the overall network connectivity is the reason for the boron anomaly behavior, which is reflected in a maximum in the glass transition temperature T_g , a minimum in the coefficient of thermal expansion CTE, dissolution rate, viscosity or molar volume [4,7, 16–21]. As shown previously in ref. [22], the properties of metaborate glasses depend not only on the degree of polymerization of the borate network but also on the cation's ability to crosslink borate units. Commonly in borate glasses, modifier cations with high ion field strength, $FS = Z/r^2$, defined by Dietzel as the cations charge divided by the square of the cation radius, lead to a higher transition temperature than borate glasses with low field strength cations [4,20]. It is known that addition of Li₂O

* Corresponding author.

E-mail address: hosamssl4@yahoo.com (H. Othman).

<https://doi.org/10.1016/j.jnoncrysol.2020.119892>

Received 8 November 2019; Received in revised form 2 January 2020; Accepted 6 January 2020

Available online 24 January 2020

0022-3093/ © 2020 Elsevier B.V. All rights reserved.

to a borate network enhances the glass forming ability, leading to high transparency glass with higher bond strength and lower melting temperature [23,24]. Introducing aluminum oxide to the glass network helps to increase the chemical stability due to the strong cross-linking capacity of trivalent Al^{3+} ions [25,26]. When adding both Al and Li to binary alkaline borate glass, chemically more resistant glasses can be obtained. The present multi technical study aims to differentiate the effect of various alkaline earth oxides and mixed alkaline earth oxides on the borate glass structure, and to correlate structural changes to selected glass properties such as glass transition temperature, density or refractive index. To reach this aim a glass series with the composition $30\text{MO}-10\text{Li}_2\text{O}-10\text{Al}_2\text{O}_3-50\text{B}_2\text{O}_3$, with $\text{M}=\text{Mg}, \text{Ca}, \text{Sr}$ and Ba was prepared and studied. For the second series, glasses $x \text{MgO}-(30-x)\text{BaO}-10\text{Li}_2\text{O}-10\text{Al}_2\text{O}_3-50\text{B}_2\text{O}_3$ were prepared to study the competing effect of Mg^{2+} versus Ba^{2+} . Both glass series were melted in duplicates, to have not only undoped glasses but also samples doped with 0.5 mol% of MnO or CuO. In the doped glasses, the probe ions were employed to study the optical and photo-luminescence properties as a function of glass composition. Also, the basicity of the prepared glasses was determined and correlated with structure and glass properties. Here, we study the effect of different types of alkaline earth oxides and the mixing of alkaline earth modifier oxides on the borate structure. We were able to correlate the glass structure and with the observed properties and gain a better understanding on the prediction of glass properties in multi component glasses.

2. Experimental methods

2.1. Glass preparation and characterization

The synthesized glass samples have the nominal composition $30\text{MO}-10\text{Li}_2\text{O}-10\text{Al}_2\text{O}_3-50\text{B}_2\text{O}_3$, with $\text{M}=\text{Mg}, \text{Ca}, \text{Sr}$ and Ba , and for the mixed glasses the composition $x\text{MgO}-(30-x)\text{BaO}-10\text{Li}_2\text{O}-10\text{Al}_2\text{O}_3-50\text{B}_2\text{O}_3$. For doped glasses, 0.5 mol% CuO or MnO substituted the respective amount of alkaline earth oxide MO. All glass samples were prepared in 20 g batches (balance accuracy is ± 0.0001 g) by melt quenching using alumina crucibles after mixing the respective amounts of H_3BO_3 (99.9%), Al_2O_3 (99.9%), Li_2CO_3 ($\sim 99.9\%$) and CuO, MnO, MgO, BaCO_3 , SrCO_3 , or CaCO_3 (all of purity 99.99% from Sigma-Aldrich); all components were dried before batching. The mixtures were heated to a final temperature of 1000–1200 °C, depending on the composition, and subsequently held for 30 min at this temperature. The melts were cast into pre-heated stainless-steel molds (300 °C) and immediately transferred to an annealing furnace. The glasses were kept at 350–450 °C for about 1 h before slowly cooling to room temperature to remove internal stress. The compositions and properties of the prepared glass samples are listed in Table 1. Samples in the first glass series are labelled according to the alkaline-earth cation and the dopant used, (e.g. Mg-MB(Cu) identifies a glass with composition 29.5 Mg-10Li₂O-10Al₂O₃-50B₂O₃-0.5CuO), whereas glasses in the second series are labelled depending on the Ba/Mg ratios and the dopant if any (e.g. 2Mg/2Ba-MB(Mn) identifies a glass with composition 14.75MgO – 14.75BaO – 10Li₂O – 10Al₂O₃ – 50B₂O₃- 0.5 MnO) (see Table 1).

Glass densities were measured by Archimedes' principle at room temperature (22 °C) using toluene as an immersion liquid. Each glass sample was measured for three times using a balance with error ± 0.0001 g. The density was calculated using the following relation: $\rho_{\text{glass}} = \frac{\rho_{\text{toluene}} \times m_{\text{air}}}{(m_{\text{air}} - m_{\text{toluene}})}$, with $\rho_{\text{toluene}} = 0.8645$ g/cm³ at room temperature, and m_{air} and m_{toluene} being the mass of glass in air and toluene, respectively. To insure the reproducibility and the accuracy of the measurements, the average value was calculated. Considering all the errors, the average error of density measurements was approximately ± 0.0055 g.cm⁻³.

Refractive indices were measured with accuracy of ± 0.0001 on polished samples with an Abbe refractometer, using monobromonaphthalene as the contact layer between the sample and prism of the refractometer.

The glass transition temperature (T_g) was obtained by differential scanning calorimetry (DSC, NETZSCH DSC 404F1) using a constant heating rate of 20 °C min⁻¹, with an instrument error of ± 2 °C, with T_g being determined from the onset of the inflection of the DSC curve.

Raman spectra were obtained in the frequency range from 100 to 2000 cm⁻¹ at 2 cm⁻¹ resolutions, using a dispersive confocal Raman microscope (Renishaw inVia) and the 488 nm laser excitation line. The estimated error in Raman band position is ca. ± 1 cm⁻¹. In cases where fluorescence from Mn- or Cu-dopants was high, other laser lines at 514.5, 633 or 785 nm or even 1064 nm were employed. All visible laser excitation lines were part of the (Renishaw inVia) system. For the NIR laser excitation at 1064 nm, a Bruker RFS100 FT-Raman spectrometer equipped with a Nd-YAG laser was used.

IR measurements were obtained on a vacuum FT-IR spectrometer (vertex80, Bruker). The spectra were collected in reflectance mode from polished samples, employing an incidence angle of ca. 11°, measuring the range from 30 to 7000 cm⁻¹ with a resolution of 2 cm⁻¹. An average of 100 scans was collected in the mid-IR (400–7000 cm⁻¹) and 200 scans in the far-IR (30–600 cm⁻¹). The average of these scans was merged, and the absorption spectra obtained were calculated through the Kramers-Kronig transformation (for more details see [1,27]) with estimated error for the position of the infrared bands of ± 2 cm⁻¹.

Analyses of optical emission and excitation behavior (PL) were performed with a spectrofluorometer equipped with double monochromators (Czerny-Turner) in excitation and emission (Fluorolog3, Horiba Jobin Yvon), using a 450 W Xe-lamp as excitation source (excitation and emission spectral resolution is 1 nm).

Absorption spectra were measured using an UV-VIS spectrometer (Lambda 950, Perkin Elmer). All measurements were carried out on polished glasses with dimensions of $\sim 0.8 \times 1.0$ cm², and 1.0–1.5 mm thickness (the thickness was measured with an accuracy of 0.001 mm).

3. Result and discussion

3.1. Basicity and optical properties of glasses

The concept of optical basicity was introduced by Duffy and Ingram as a measure of the electron donor power of glasses [15,16,28]. The optical basicity is, for example, related to the ligand field strength that transition metal ions such as copper or manganese ions experience in a glass [13,14], but also to the average oxygen polarizability and, thus, to the refractive index and optical band gap of a glass [29–31].

The theoretical optical basicity, Λ_{th} , of the prepared glasses was calculated from the composition using the following equation [16,28,32–34]:

$$\Lambda_{th} = X(AO_{a/2})\Lambda(AO_{a/2}) + X(BO_{b/2})\Lambda(BO_{b/2}) + \dots \quad (1)$$

where Λ is the optical basicity and X the oxygen equivalent fraction for each oxide [6]. The oxygen equivalent fraction differs from the molar fraction in so far, as it also accounts for the number of oxygen atoms per oxide. Table 1 lists the average or theoretical optical basicity values of the studied glasses. The following basicity values for the simple oxides were used in these calculations: $\Lambda(\text{Li}_2\text{O})=0.81$; $\Lambda(\text{MgO}^{(6)})=0.61$; $\Lambda(\text{CaO})=1$; $\Lambda(\text{SrO})=1.08$; $\Lambda(\text{BaO})=1.22$; $\Lambda(\text{Al}_2\text{O}_3^{(4)})=0.6$; and $\Lambda(\text{B}_2\text{O}_3)=0.24^{(4)}$ or $0.4^{(3)}$ [28,34,35], with superscripts in brackets denoting the coordination number of the relevant cations. We assume four-fold coordination for Al^{3+} [36,37,38], and a mixed three and four-fold coordination for B^{3+} . We calculated, therefore, the theoretical basicity using an averaged value of $\Lambda(\text{B}_2\text{O}_3)=0.35$ ($1\text{B}_4:2\text{B}_3$ with B_3 and B_4 standing for the fraction of tetrahedral and trigonal borate units) or using the value of $\Lambda(\text{B}_2\text{O}_3)=0.4$ for trigonal borate units only.

Another way to determine the optical basicity is based on refractive index measurements, since the optical basicity relates directly to the oxygen polarizability. In this approach, the average molar electronic polarizability of a glass, α_m , is determined from the Lorentz-Lorenz equation:

Table 1

Nominal compositions of the investigated glasses, and some of their properties: glass transition temperature (T_g), density, molar volume (V_m), refractive index at 585 nm (n_d), position of excitation maximum of Mn^{2+} ions (EX_{max}). Optical basicity values were derived from composition (Λ_{th}), refractive index (n_d) and oxygen polarizability measurements (Λ_n), and by using Mn^{2+} as a probe ion (Λ_{Mn}). For details see text.

Sample	T_g (°C)	Density (g/cm ³)	V_m (cm ³ /mol)	n_d	EX_{max} (cm ⁻¹)	Optical basicity		
						Λ_{th}	Λ_n	Λ_{Mn}
Error:	± 2	± 0.005		± 0.0001				
29.5 MO – 10Li₂O – 10 Al₂O₃ – 50 B₂O₃ – 0.5 CuO (M=Mg, Ca, Sr, Ba), melted in air								
Mg-MB(Cu)	538	2.43	24.81	1.5473	–	0.456	0.474	–
Ca-MB(Cu)	520	2.60	24.97	1.5928	–	0.498	0.520	–
Sr-MB(Cu)	511	3.05	25.89	1.6055	–	0.511	0.544	–
Ba-MB(Cu)	502	3.38	27.70	1.6209	–	0.527	0.580	–
29.5 MO – 10Li₂O – 10 Al₂O₃ – 50 B₂O₃ – 0.5 MnO (M=Mg, Ca, Sr, Ba) melted in air								
Mg-MB(Mn)	537	2.42	24.89	1.5455	24290	0.456	0.475	0.597
Ca-MB(Mn)	519	2.59	25.07	1.5939	24073	0.498	0.527	0.654
Sr-MB(Mn)	510	3.04	25.96	1.6041	23987	0.511	0.545	0.677
Ba-MB(Mn)	503	3.37	27.77	1.6201	23952	0.527	0.582	0.686
xMgO – (30-x)BaO – 10Li₂O – 10 Al₂O₃ – 50 B₂O₃ (x=0, 7.5, 15, 22.5) undoped								
4Mg/0Ba-MB	535	2.42	24.83	1.5513	–	0.455	0.483	–
3Mg/1Ba-MB	525	2.67	25.68	1.5663	–	0.474	0.509	–
2Mg/2Ba-MB	514	2.95	26.11	1.5821	–	0.492	0.516	–
1Mg/3Ba-MB	506	3.25	26.31	1.6022	–	0.510	0.520	–
0Mg/4Ba-MB	501	3.37	27.93	1.6173	–	0.528	0.583	–
xMgO – (29.5-x)BaO – 10Li₂O – 10 Al₂O₃ – 50 B₂O₃ – 0.5 MnO (x=0, 7.25, 14.75, 22.25)								
3Mg/1Ba-MB(Mn)	526	2.68	25.53	1.5722	24201	0.475	0.513	0.621
2Mg/2Ba-MB(Mn)	517	2.94	26.16	1.5901	24120	0.492	0.533	0.642
1Mg/3Ba-MB(Mn)	509	3.11	27.45	1.5997	24073	0.508	0.570	0.654

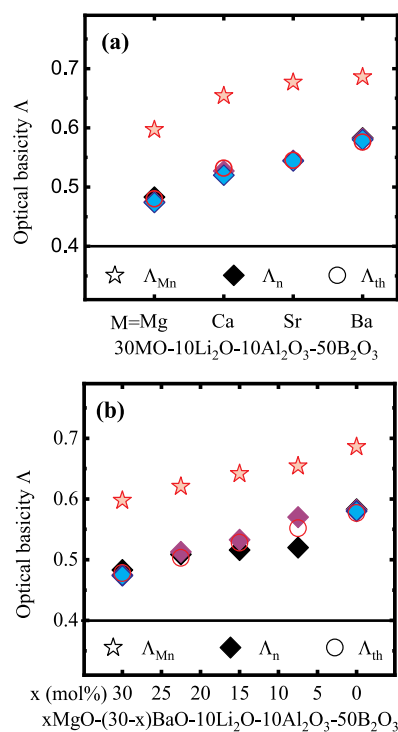


Fig. 1. Optical basicity values of (a) single alkaline earth borate glasses and (b) the mixed Mg/Ba borate glasses. Diamonds: Λ_n basicity values from refractive index (blue for glasses doped with Cu, purple for glasses doped with Mn, black for undoped glasses); open circles: theoretical values, Λ_{th} , from composition (red, using $\Lambda(B_2O_3)=0.35$ based on $N_4=0.33$), Λ_{Mn} basicity values using Mn^{2+} as probe ions (red stars). The symbol size is larger than the error bars. (For interpretation of the references to color in this figure legend, the reader is referred to the web version of this article.)

$$\alpha_m = \frac{3V_m}{4\pi N} \cdot \frac{n^2 - 1}{n^2 + 2} \quad (2)$$

Where N_A is the Avogadro number and n the refractive index of the glass. V_m is the molar volume of the glasses calculated using the

relation $V_m = \frac{M_w}{\rho}$, with M_w being the molecular weight and ρ the glass density. The oxygen polarizability is obtained by first subtracting the cation polarizabilities of the multi component material from the overall polarizability α_m , and then dividing the obtained value by the number of oxygen atoms per glass chemical formula [28]:

$$\alpha_{O^{2-}} = \frac{\alpha_m - \alpha(\sum C^{n+})}{\text{number of O per glass formula}} \quad (3)$$

The cation polarizabilities were taken from literature with $\alpha(Li^+) = 0.024 \text{ \AA}^3$, $\alpha(Al^{3+}) = 0.054 \text{ \AA}^3$, $\alpha(B^{3+}) = 0.002 \text{ \AA}^3$, $\alpha(Mg^{2+}) = 0.094 \text{ \AA}^3$, $\alpha(Ca^{2+}) = 0.469 \text{ \AA}^3$, $\alpha(Sr^{2+}) = 0.861 \text{ \AA}^3$, $\alpha(Ba^{2+}) = 1.595 \text{ \AA}^3$, $\alpha(Mn^{2+}) = 0.544 \text{ \AA}^3$, and $\alpha(Cu^{2+}) = 0.437 \text{ \AA}^3$ [29,38,39].

The average oxygen polarizability $\alpha_{O^{2-}}$ relates to the theoretical optical basicity via the following empirical formula [28–31,40]:

$$\Lambda_{th} = 1.67 \left(1 - \frac{1}{\alpha_{O^{2-}}} \right) \quad (4)$$

The optical basicity was also experimentally evaluated from the position of the maximum of the excitation peak of the probe ion Mn^{2+} , using the following equation [13,15]:

$$\Lambda_{site} = \frac{\nu_{s \rightarrow G}^f - \nu_{s \rightarrow G}}{2.56 \cdot K \cdot \nu_{s \rightarrow G}^f} \quad (5)$$

where K is a constant specific to a particular metal ion (*i.e.*, $K=0.0688$ for Mn^{2+}), and $\nu_{s \rightarrow G}^f$ is the frequency of the free (uncomplexed) Mn^{2+} ions (26846 cm^{-1}). Values for $\nu_{s \rightarrow G}$ were determined from photo-luminescence measurements (excitation maximum values, EX_{max} , in Table 1).

For all glasses, the measured refractive index values and the calculated optical basicity values are listed in Table 1. The variations in the optical basicities for the different alkaline earth cations are depicted in Fig. 1a, while Fig. 1b plots the optical basicity values for the mixed Mg/Ba-borate glass series. As expected, the basicity values decrease from BaO to MgO, with SrO and CaO giving intermediate values. Since different basicity values of the studied glasses are given in the literature for trigonal [B₃] or tetrahedral [B₄] borate units, basicity values depend on the assumed borate speciation. Here, we find in Fig. 1a and b that the calculated theoretical optical basicity (Λ_{th}) agrees very well with the one determined from refractive index values (Λ_n) only for $\Lambda(B_2O_3)=0.35$, *i.e.* by assuming a B₃:B₄

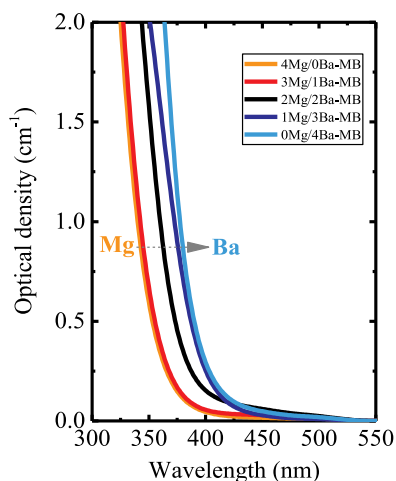


Fig. 2. Optical absorption spectra of undoped glasses, melted in air for the series $x\text{MgO}-(30-x)\text{BaO}-10\text{Li}_2\text{O}-10\text{Al}_2\text{O}_3-50\text{B}_2\text{O}_3$. The spectra are normalized to a sample thickness of $d=1$ cm.

ratio of 2:1 ($N_4 = B_4/(B_4 + B_3) = 0.33$, slightly lower than the IR results of the Mg-poor glasses; see Sections 3.3 and 4).

The basicity values determined by using Mn^{2+} as a probe ion, Λ_{Mn} , are consistently higher than the theoretical values, Λ_{th} , and those obtained from refractive index measurements, Λ_{n} . This result indicates that Mn^{2+} ions seek out specifically higher basicity sites than those of average basicity, in agreement with earlier papers for Pb^{2+} , Tl^+ and Mn^{2+} probe ions in borate and phosphate glasses [13,41–44].

UV-VIS spectra of the mixed alkaline earth undoped glass series $x\text{MgO}-(30-x)\text{BaO}-10\text{Li}_2\text{O}-10\text{Al}_2\text{O}_3-50\text{B}_2\text{O}_3$ ($x=0, 7.5, 15, 22.5$) are shown in Fig. 2. As expected the UV cut-off shifts to lower energy with increasing BaO content; hence by increasing optical basicity.

Mn^{2+} ions, contrary to the Mn^{3+} species, give rise to photoluminescence. Mn^{2+} excitation (Ex_{max}) and emission (Em_{max}) spectra were measured, respectively, at the maximum of the emission and excitation lines, for glasses in the mixed alkaline earth series and for the two Mn-bearing end-members in the single alkaline-earth series (Mg- and Ba-MB(Mn)). Both Em_{max} and Ex_{max} intensities increase with increasing Mg/Ba ratio (Fig. 3), and higher intensities correlate with a decreasing optical basicity of glass (see Table 1). This indicates that a higher fraction of Mn^{2+} ions is stabilized in low basicity glasses. In turn, glasses having higher optical basicities stabilize better the higher oxidized species Mn^{3+} which provide a strong absorption in the visible region (giving to the glass, indeed, a pink to dark purple colour); thus, further decreasing the photoluminescence intensities. The maximum excitation intensity shifts toward lower energy with increasing optical basicity, see Table 1 and Fig. 3b (for the normalized excitation intensity). A similar behaviour is seen for the single alkaline earth glasses, where the photoluminescence intensities decrease in the order $\text{Mg} > \text{Ca} > \text{Sr} > \text{Ba}$ (not shown; see Table 1 for excitation band positions).

3.2. Raman spectroscopy

The Raman spectra of the glass samples are shown in Fig. 4. Due to fluorescence from Cu^+ , Mn^{2+} ions and impurities, the raw spectra (Fig. 4a, c) needed background correction (Fig. 4b, d) to allow for an assessment of the various borate peaks. Fig. 4a, b shows the effect of different alkaline earth ions on the borate Raman features and Fig. 4c, d the corresponding effect of Mg-Ba mixing. Since Cu^+ and Mn^{2+} ions are excited at different wavelengths, the laser excitation line was varied for the best statistics of the Raman spectra, resulting in a different slope of the respective remaining fluorescence background. Analysis based on band assignments that are discussed in detail in earlier Raman studies, such as [2,4–6,22,45–49] and references therein.

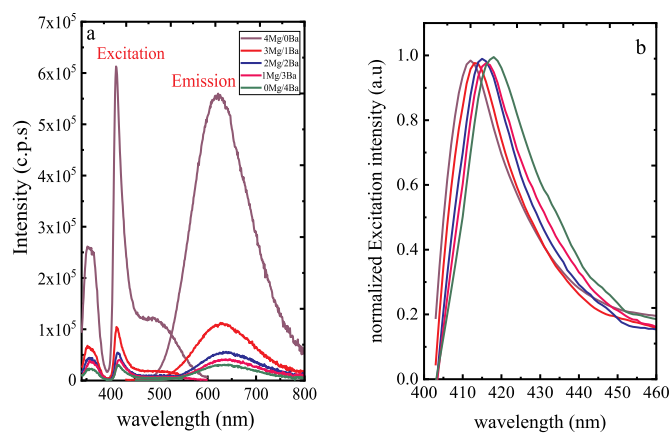


Fig. 3. (a) Mn^{2+} excitation ($\lambda_{\text{em}} = 623$ nm) and emission ($\lambda_{\text{ex}} = 415$ nm) spectra for mixed alkaline Mn-doped glasses of the $x\text{MgO}-(29.5-x)\text{BaO}-10\text{Li}_2\text{O}-10\text{Al}_2\text{O}_3-50\text{B}_2\text{O}_3$ series doped with 0.5 MnO (with a resolution of 1 nm), and (b) Plot of the respective excitation spectra normalized to the maximum of the peak. (For interpretation of color in this figure, the reader is referred to the web version of this article.)

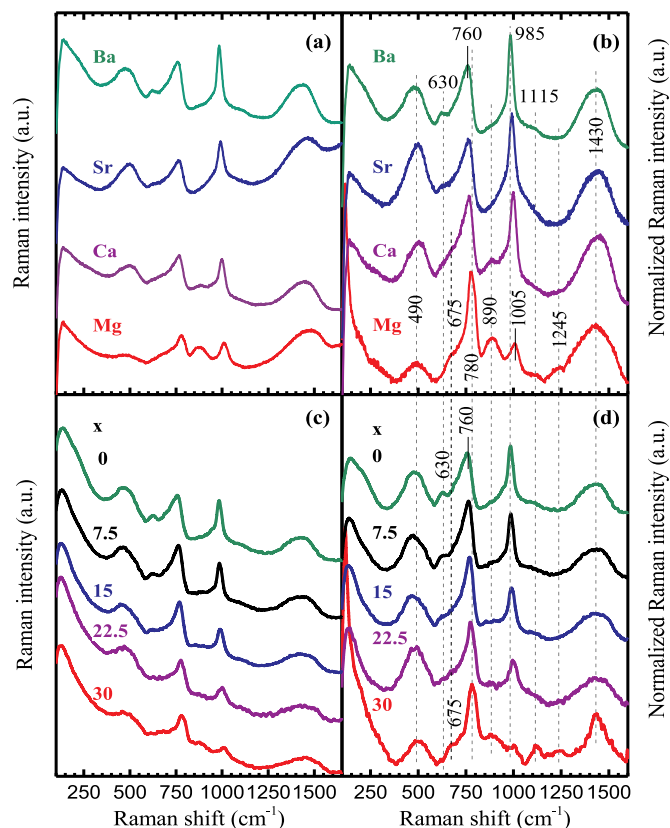


Fig. 4. Raman spectra as measured (a, c) and after background correction (b, d) due different fluorescence backgrounds of (a, c). Cu-doped glasses of the $x\text{MgO}-10\text{Li}_2\text{O}-10\text{Al}_2\text{O}_3-50\text{B}_2\text{O}_3$ series with $M = \text{Mg}, \text{Ca}, \text{Sr}$ and Ba (Raman excitation at 488 nm) are shown in (a, c), and undoped glasses $x\text{MgO}-(30-x)\text{BaO}-10\text{Li}_2\text{O}-10\text{Al}_2\text{O}_3-50\text{B}_2\text{O}_3$ (Raman excitation at 1064 nm) are shown in (b, d). All spectra are normalized to the maximum intensity and off-set in regard to the y-axis for clarity.

The intense sharp contribution around $985\text{--}1005\text{ cm}^{-1}$ is due to asymmetric stretching modes of tetrahedral borate groups [2,6,47,49], while the broad envelop peaking at about 1430 cm^{-1} is attributed to boron–oxygen stretching modes in trigonal borate entities including B-O^- stretching in metaborate triangles $\text{B}\text{O}_2\text{O}^-$, where O^- = bridging oxygen atom [2,4,46–49]. The broadness of this band envelop reflects

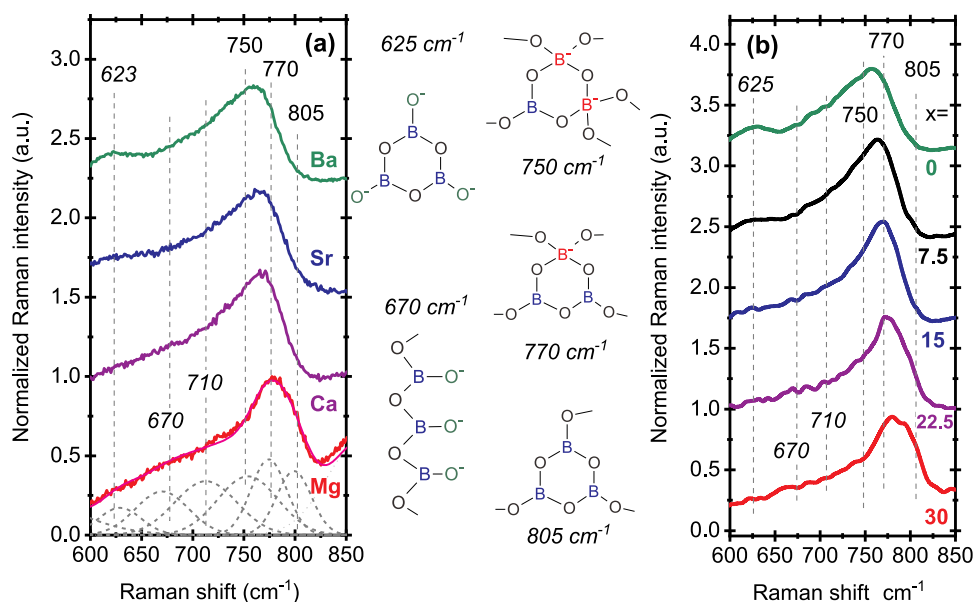


Fig. 5. Enlarged spectral range from 600 to 850 cm^{-1} of the Raman spectra depicted in Fig. 4b and d, including one example of band deconvolution for the Mg-MB glass. In the center, the schematics display the various borate superstructural units that contribute with their ring breathing mode (805, 770, 750, 625 cm^{-1}) and deformation modes (670 cm^{-1}) to the observed Raman signal.

the different band positions of borate triangles inside and outside ring-structures, as well as the presence of borate trigonal units with only bridging or non-bridging oxygen atoms [4,22]. The strong band around 760–780 cm^{-1} is attributed to ring breathing vibrations of six-membered rings containing two trigonal BO_3^0 and one tetrahedral $[\text{B}\text{O}_4]^-$ unit ($\sim 780 \text{ cm}^{-1}$), or one trigonal BO_3^0 and two tetrahedral $[\text{B}\text{O}_4]^-$ borate units ($\sim 750 \text{ cm}^{-1}$) [2,4,22,45–50]. Weaker Raman bands arise from bending modes of metaborate chains, $(\text{B}\text{O}_3^-)_n$, at 675 cm^{-1} , the breathing mode of metaborate rings, $(\text{B}_3\text{O}_3^3)^{3-}$, at 630 cm^{-1} , and borate bending modes involving $[\text{B}\text{O}_4]^-$ tetrahedra in medium-range order units as well as Al-O-B bonds near 490 cm^{-1} [2,6,22,46–50].

The spectrum of the Mg-MB and Mg-rich glasses in Fig. 4a and 4b shows a contribution at 890 cm^{-1} , which appears weakly also in the Ca-MB spectrum (Fig. 4a). Crystalline magnesium-pyroboration ($2\text{MgO}\cdot\text{B}_2\text{O}_3$) and magnesium-orthoborate ($3\text{MgO}\cdot\text{B}_2\text{O}_3$) compounds show strong and sharp Raman bands at 850 and 930 cm^{-1} , respectively [46]. The 850 cm^{-1} band is due to the symmetric stretching of the B-O-B bridge in pyroboration groups, $\text{B}_2\text{O}_5^{4-}$, and the 930 cm^{-1} corresponds to the symmetric stretching of the orthoborate unit, BO_3^{3-} [46]. The corresponding Raman bands in Mg-borate glasses were measured at 840–850 cm^{-1} for pyroboration units and 930–945 cm^{-1} for orthoborate units [4,46]. Therefore, the broad 880 cm^{-1} band in Fig. 4b indicates the coexistence of small amounts of pyroboration and orthoborate units in the Mg-MB glass. Further evidence for the presence of pyroboration units in this glass is provided by the weak shoulder at about 1245 cm^{-1} corresponding to the symmetric stretching of the terminal B-O $^-$ bonds of the $\text{B}_2\text{O}_5^{4-}$ unit (Fig. 4b). Another weak shoulder at 1100 cm^{-1} can be assigned to B-O stretching modes of tetrahedral borate groups connected to trigonal borates with non-bridging oxygen atoms or tetrahedral borate in diborate entities [4–6,22,48]. A diborate superstructural unit consists of two corner-sharing $[\text{B}\text{O}_4]^-$ tetrahedral units which participate in two three-membered rings, each ring containing additionally one BO_3 group [1]. The low frequency scattering below 300 cm^{-1} arises from diverse network deformation modes and merges into the boson peak.

3.2.1. Effect of alkaline earth oxides on the Raman spectra

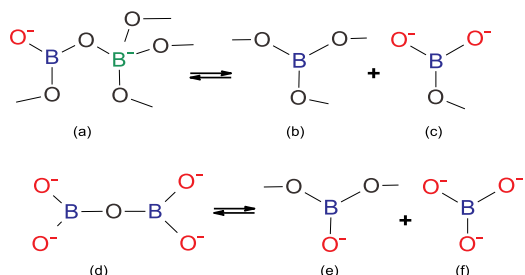
We focus here on some Raman bands which exhibit a profound dependence on the type of alkaline earth cation. As observed in Fig. 4a, the maximum of the sharp band due to $[\text{B}\text{O}_4]^-$ tetrahedral units downshifts with increasing mass of the alkaline earth cation from 1005 cm^{-1} for M=Mg to 985 cm^{-1} for M=Ba. Furthermore, this band gains relative intensity in the direction $\text{Mg} < \text{Ca} < \text{Sr} < \text{Ba}$, reflecting an

increasing fraction of tetrahedral borate units for the glasses with heavier modifier ions. This result is in agreement with earlier findings for binary alkaline earth borate glasses $y\text{MO}\cdot(1-y)\text{B}_2\text{O}_3$ [4].

The effect of alkaline earth cation on the relative population of $[\text{B}\text{O}_4]^-$ tetrahedra is also manifested in the progressive shift of the ring breathing mode from 780 cm^{-1} for M=Mg to 760 cm^{-1} for M=Ba, indicating an increasing number of three-membered rings with two $[\text{B}\text{O}_4]^-$ tetrahedra in the same direction. Fig. 5a shows enlarged the 600–850 cm^{-1} region which includes the breathing mode activity of four different 3-membered borate rings with varying BO_3 , $[\text{B}\text{O}_4]^-$ and $\text{B}\text{O}_2\text{O}^-$ entities (see schematic in Fig. 5). Superposition of five to six bands prevents any precise quantification; however, the observed shift in the apparent band maximum with decreasing field strength of the modifier alkaline earth cation from about 780 cm^{-1} for M=Mg to 760 cm^{-1} for M=Ba is significant. From the shown example of deconvolution for the M=Mg spectrum it is apparent that the Mg-rich glasses (Fig. 5a and b) contain a noteworthy number of boroxol-rings (ring breathing mode at 805 cm^{-1} [2,4]), which are absent in the Ba-rich glasses. For the Ca- and Sr-MB glasses the maximum shifts to 767 and 765 cm^{-1} , reflecting on a high number of rings with 1 $[\text{B}\text{O}_4]^-$ metaborate entity, while the further shift to 760 cm^{-1} for the Ba-MB glass reflects on the presence of rings with 2 $[\text{B}\text{O}_4]^-$ metaborate entities. Thus, the relative intensity of the ring modes with 2 $[\text{B}\text{O}_4]^-$ tetrahedra and 1 neutral BO_3 unit (755 cm^{-1}) increases with decreasing field strength of the alkaline earth cation, i.e. in the order $\text{Mg} < \text{Ca} < \text{Sr} < \text{Ba}$.

The shoulder at 675 cm^{-1} is typical for B-O-B bending modes of chain type metaborate units [49], which is best separated in the spectrum of the Mg-MB glass (Figs. 4b, 5a). On the other hand, the breathing modes of metaborate rings give their strongest Raman band from about 603 cm^{-1} ($\text{Cs}_2\text{O}\cdot\text{B}_2\text{O}_3$ [49,51]) to about 635 cm^{-1} ($\text{BaO}\cdot\text{B}_2\text{O}_3$ [4,49]). Therefore, the M=Ba end of the glass series appears to have a preference for metaborate rings (Fig. 4a), while metaborate chains are present in the M=Mg glass. As noted above, the M=Mg glass structure involves also boroxol rings as indicated by the band deconvoluted at 805 cm^{-1} (Fig. 5a), in agreement with earlier findings in binary Mg-borate glasses [4,46]. These neutral boroxol rings seems to coexist with the highly charged, and highly depolymerized pyroboration $\text{B}_2\text{O}_5^{4-}$ and orthoborate BO_3^{3-} entities giving rise to the 890 cm^{-1} band in Fig. 4a. This suggests that the high field strength Mg^{2+} ion induce the disproportionation of the glass network. The same process was also suggested for other glasses discussed in the literature [4,10,22,46,52], where Mg^{2+} , Zn^{2+} but also Ca^{2+} ions foster the disproportionation of

the glass network in highly charged groups with several non-bridging oxygen atoms to form their coordination sphere and to polymerized units that are needed to fulfill the requirements of stoichiometry and charge balance [4,10,46]. This behavior of metaborate glasses can be described by the following disproportionation equilibria depicted in Schematic 1:



Schematic 1. Disproportionation of metaborate $\text{B}\text{O}_2\text{O}^-$ and $[\text{B}\text{O}_4]^-$ units into (a) neutral BO_3 and (b) pyroborate $\text{B}_2\text{O}_4^{2-}$ (c), and disproportionation of pyroborate $\text{B}_2\text{O}_4^{2-}$ (d) into metaborate $\text{B}\text{O}_2\text{O}^-$ (e) and orthoborate BO_3^{3-} (f).

Indeed, the $\text{M}=\text{Mg}$ glass was found to have the strongest signatures of metaborate chains ($\text{B}\text{O}_2\text{O}^-$ -chains at 675 cm^{-1}), boroxol rings ($3\text{B}\text{O}_3$, 805 cm^{-1}), pyroborate and orthoborate units (convoluted at 890 cm^{-1}), and the weakest signature for $[\text{B}\text{O}_4]^-$ units (1005 cm^{-1}), just as expected for the alkaline earth cation with the highest field strength.

3.2.2. Raman spectra of mixed Mg-Ba-borate glasses

Figs. 4d and 5b show the background corrected Raman spectra of mixed Mg-Ba-borate glasses. The end members of this glass series, $4\text{Mg}/0\text{Ba}$ and $0\text{Mg}/4\text{Ba}$, corresponding to the Mg- and Ba-MB glass respectively, were derived from a different melting cycle and are doped differently than the spectra of the Mg- and Ba-MB glasses shown in Figs. 4b and 5a. Similar spectra are expected for glasses of similar composition, and overall we see a good reproducibility for analogue glasses from different melting cycles. Slight variations in the spectral form of the Mg-MB glasses might reflect on the different background correction needed for spectra taken with 488 nm and 1064 nm Raman excitation. The near infrared excitation line was necessary for the undoped glasses with their low impurity levels for which fluorescence was much more detrimental when excited in the visible wavelength range than it was for the doped glasses. Though background correction might account for some variations between samples of similar composition, isomerization should also be considered to occur for variations of the melting and annealing temperatures, which, in turn, will induce shifts in the equilibrium depicted in Schematic 1. Evidence for isomerism within glass fragments from the same melt, but with varying fictive temperatures has been observed in manganese-strontium orthoborate glasses as described in reference [5].

In accordance with the discussion in 3.2.1, the Raman spectrum of the Mg-MB end member shows a high number of trigonal borate units, including neutral BO_3^0 entities (shoulder at 800 cm^{-1} of the band peaking at 770 cm^{-1}) and of doubly negatively charged pyroborate $\text{B}_2\text{O}_4^{2-}$ dimers (contribution at 890 and 1275 cm^{-1}). As discussed in the previous section, the $\text{B}-\text{O}^-$ stretching mode of orthoborates would add contribution to the 890 cm^{-1} band which appears of much weaker intensity relative to the corresponding signal in the Cu-doped Mg-MB glass discussed earlier.

As Ba^{2+} substitutes for Mg^{2+} , the signature of the $[\text{BO}_{4/2}]^-$ band at about 985 cm^{-1} increases steadily in intensity. This trend is consistent with the gradual shift in the position of the breathing mode of 3-membered rings with $[\text{B}\text{O}_4]^-$ tetrahedral from 780 cm^{-1} to 760 cm^{-1} as Mg^{2+} is replaced by Ba^{2+} , reflecting on a higher number of borate rings with two $[\text{B}\text{O}_4]^-$ tetrahedral. Thus, substituting Mg^{2+} by Ba^{2+} increases progressively the number of tetrahedral borate groups.

The signature of metaborate chains at 675 cm^{-1} is clearly observed

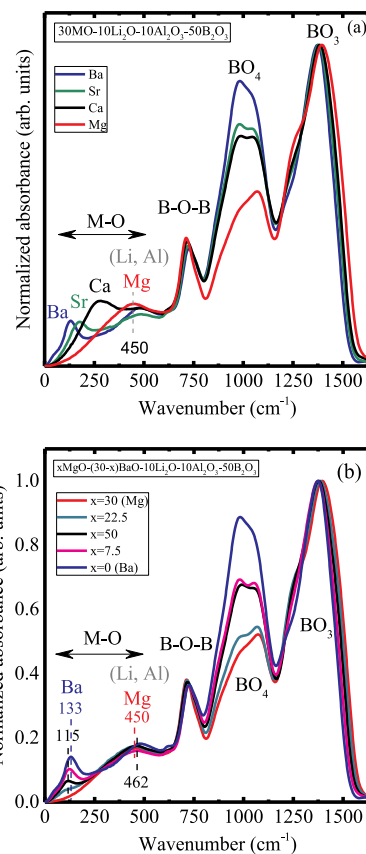


Fig. 6. IR spectra of (a) the alkaline-earth series $30\text{MO}-10\text{Li}_2\text{O}-10\text{Al}_2\text{O}_3-50\text{B}_2\text{O}_3$ with $\text{M}=\text{Mg, Ca, Sr}$ and Ba , and (b) the mixed $x\text{MgO}-(30-x)\text{BaO}-10\text{Li}_2\text{O}-10\text{Al}_2\text{O}_3-50\text{B}_2\text{O}_3$ series. The best spectra were obtained from the largest samples, thus the displayed spectra are: for (a) Mg-MB(Cu), Ca-MB(Mn), Sr-MB(Mn) and Ba-MB (undoped); for (b) the same end members were used together with the undoped mixed glasses and the sample $3\text{Mg}/1\text{Ba}-\text{MB}(\text{Mn})$.

for the Mg-MB end member ($x=30$ in Fig. 4d) and is gradually replaced by the metaborate ring signature at 630 cm^{-1} towards the Ba-MB end member ($x=0$ in Fig. 4d).

3.3. Infrared spectra

Fig. 6 shows the infrared spectra of the two-glass series. Since the dopant concentration of $0.5\text{ mol}\%$ or 5000 ppm can be neglected in terms of its structural impact, we selected only the best quality spectra for display. Four band systems can be distinguished; the two high intensity ones around $800-1200\text{ cm}^{-1}$ and $1200-1600\text{ cm}^{-1}$ arise from the B-O stretching modes in tetrahedral and trigonal borate groups, respectively, while the absorption peak observed around 715 cm^{-1} is assigned to the bending vibrations of various borate species [1,2,4,10,22,46]. The cation-site vibrations are active in the far IR region with the corresponding frequency $\nu(\text{M}-\text{O})$ decreasing with the mass of metal cation [1,2,4,22,53]. For the studied glasses the $\nu(\text{M}-\text{O})$ frequency varies as follows: Ba^{2+} (131 cm^{-1}) < Sr^{2+} (175 cm^{-1}) < Ca^{2+} (282 cm^{-1}) < Mg^{2+} (ca. 450 cm^{-1}) in line with results obtained for binary alkaline earth borate glasses [4].

As seen in Fig. 6, the intensity of the BO_4 envelope relative to that of BO_3 increases in the order $\text{Mg}^{2+} < \text{Ca}^{2+} < \text{Sr}^{2+} < \text{Ba}^{2+}$, i.e. it follows the same trend as observed above by Raman spectroscopy. Also, the BO_4 and BO_3 envelopes appear to consist of contributions from several bands, due to different network connectivity like ring-, chain-type and other superstructural units. In the case of BO_3 trigonal units, varying numbers of bridging and non-bridging oxygen atoms (from poly- to ortho-borate) add various contributions.

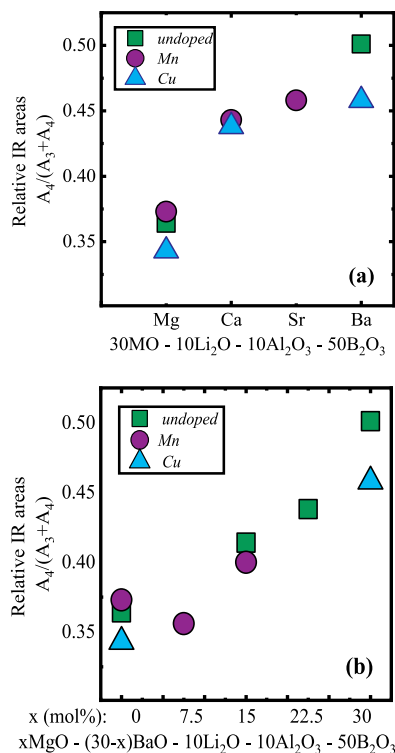


Fig. 7. Relative integrated IR intensity of BO_4 units for the prepared undoped and doped (a) single alkaline-earth borate glasses $30\text{MO}-10\text{Li}_2\text{O}-10\text{Al}_2\text{O}_3-50\text{B}_2\text{O}_3$ with $\text{M}=\text{Mg}, \text{Ca}, \text{Sr}$ and Ba , and (b) the mixed alkaline-earth $x\text{MgO}-(30-x)\text{BaO}-10\text{Li}_2\text{O}-10\text{Al}_2\text{O}_3-50\text{B}_2\text{O}_3$ borate glass series. The size of the points is exceeding the error bars.

The IR data were used to calculate the relative integrated intensity corresponding to BO_4 units as $A_4/(A_3 + A_4)$, where A_4 is the integrated intensity between 805 and 1160 cm^{-1} attributed to BO_4 units and A_3 is the integrated intensity between 1160 and 1625 cm^{-1} corresponding to BO_3 units. The relative integrated intensity $A_4/(A_3 + A_4)$ is depicted in Fig. 7 and listed in Table 2. It can be noticed that the ratio $A_4/(A_3 + A_4)$, which is proportional to the fraction of four-coordinate boron atoms N_4 , increases from Mg to Ba. This trend in N_4 reflects the disproportionation reaction in Schematic 1, which leads to the destruction of BO_4 units in favor of borate triangular units with NBOs in the presence of high field strength cations like Mg^{2+} . The small variations between the differently doped glasses of the same nominal composition

reflect variations in the equilibrium of tetrahedral and trigonal metaborate units and small variations in the melting parameters of the various melting cycles. The variations in N_4 for the two glass series, being higher for $\text{Ba} > \text{Sr} > \text{Ca}$ and being lowest for Mg, are similar to those observed for the calculated optical basicity values discussed earlier in Section 3.1.

3.3.1. Far Infrared spectra and the force constant $F_{\text{M-O}}$

It is known that cation-oxygen vibration bands occur around 400 cm^{-1} for Mg, 280 cm^{-1} for Ca, 200 cm^{-1} for Sr and around 180 cm^{-1} for Ba containing metaborate glasses and at slightly lower frequencies for metaphosphate glasses [4,22,53]. The cation-site vibration frequency depends strongly on the mass of the cation, gives direct insights on the strength of the metal-oxygen bonding, and it can often be related to glass properties such as mechanical strength and the glass transition temperature T_g [4,22]. The force constant of the metal ion-site vibrations in glass, $F_{\text{M-O}}$, can be calculated using Eq. (6) [4]:

$$F_{\text{M-O}} = 4\pi^2 c^2 \mu \nu^2 \quad (6)$$

where ν is the M-O vibration frequency measured in the far-IR, c is the speed of light and μ is the reduced mass of the cation-site vibration that could be calculated as follows for octahedral sites [4,54]:

$$\mu = \frac{m_{\text{C}} * m_{\text{O}}}{m_{\text{C}} + 2m_{\text{O}}} \quad (7)$$

where m_{C} is the mass of metal cation and m_{O} is the mass of oxygen. See Table 2 for a listing of $F_{\text{M-O}}$ values.

Fig. 8a compares the positions of the maxima of the cation-oxygen vibration bands in the far-IR for the alkaline earth cations of the lithium-alumoborate glasses of this study with the frequencies observed for binary alkaline earth borate glasses from ref. [4]. The frequencies of the cation motion bands of the Li-alumoborate glasses of this study are lower than those in the binary metaborate glasses for the alkaline earth ions of lower cation field strength (FS), while only the Mg-glass shows a higher frequency than the Li- and Al-oxide free glasses. The motion of Li^+ and Al^{3+} cations against their sites gives bands overlapping slightly with the band of Mg^{2+} ions; therefore, the band position of Mg-O cannot be determined with the same accuracy as for Ca^{2+} , Sr^{2+} or Ba^{2+} . However, Fig. 8a clearly shows that the higher the difference in the field strength, the more is the cation frequency shifted to lower energies compared to the binary metaborate glass. For the mixed Mg/Ba-MB glasses (Fig. 8b), we plot only the Ba^{2+} frequency since the Mg^{2+} motion band overlaps with the Li and Al bands. A linear decrease of $\nu(\text{Ba-O})$ is found as Mg^{2+} substitutes for Ba^{2+} in the mixed glass series. This agrees well with earlier studies, that in mixed modifier oxide glasses the far infrared band of the cation with the lower field strength

Table 2

IR parameter such as the relative integrated intensity of the absorption envelopes due to tetrahedral (A_4) and trigonal (A_3) borate units, the estimated fraction of boron atoms in tetrahedral coordination (N_4), and the force constant $F_{\text{M-O}}$ of the Mg-O, Ca-O and Ba-O bonding calculated from the frequency of the corresponding cation motions band, $\nu(\text{M-O})$.

Sample	A_4	A_3	N_4	N_4 (for composition) ref.	$\nu_{\text{M-O}} (\pm 2)$ cm^{-1}	$F_{\text{M-O}}$ dyn/sec
4Mg/0Ba-MB	160	279	0.364	0.2 (50B-50Mg) [22]	464	87615 (u)
	148	283	0.343		450	82408 (Cu)
	164	276	0.373		447	81313 (Mn)
Ca-MB	199	255	0.438	0.4 (50B-50Ca) [4,22]	289	43783 (Cu)
	205	258	0.443		282	41687 (Mn)
	212	251	0.458		176	21390 (Mn)
Sr-MB	236	235	0.501	0.38 (53B-47Sr) [4,22]	131	13123 (u)
Ba-MB	200	237	0.458	0.34 (50B-50Ba) [4,22]	134	13729 (Cu)
1Mg/3Ba-MB	194	249	0.438	0.52 (50B-30Ba-20Pb) [14]	$\nu_{\text{Ba-O}}$	$F_{\text{Ba-O}}$
	205	255	0.446		124	11756 (u)
	184	260	0.414		121	11194 (Mn)
2Mg/2Ba-MB	184	260	0.414		115	10112 (u)
3Mg/1Ba-MB	152	275	0.356		102	7955 (Mn)

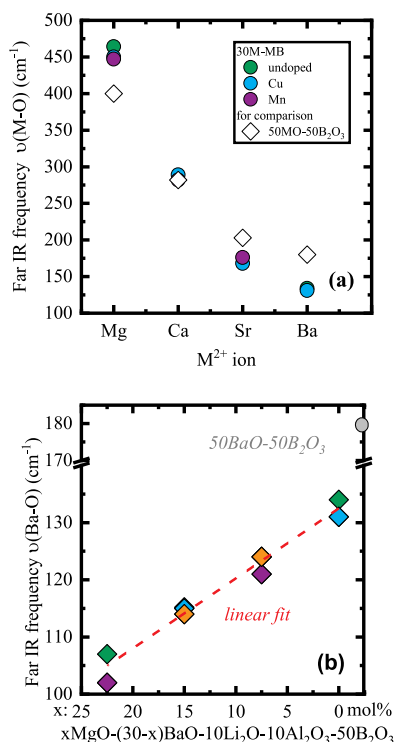


Fig. 8. Variations in the M-O vibration frequency in the far IR with (a) variation of the alkaline earth cation in the single alkaline-earth borate glasses 30MO-10Li₂O-10Al₂O₃-50B₂O₃ with M = Mg, Ca, Sr and Ba, and (b) the mixed alkaline-earth x MgO-(30-x) BaO-10Li₂O-10Al₂O₃-50B₂O₃ borate glass series, only the Ba-O frequency is shown since the Mg-O band overlaps with Li-O and Al-O vibration bands. For comparison, the values for the M-O vibration frequencies are included for single metaborate glasses 50MO-50B₂O₃: open diamonds in (a) and grey circle in (b) [4]. The accuracy of 2 cm^{-1} is lower than point size.

shifts further to lower wavelengths, while the infrared bands of the high field cation moves to higher energies relatively to the single modifier glasses [55–59].

The linear shift in band position of the Ba-O vibration found here for the lithium aluminoborate glasses is a structural reflection of the mixed modifier effect, as demonstrated also in Fig. 9. Here, the measured far-IR spectra of the mixed Mg/Ba glasses are compared with the calculated far-IR spectra based on the weighted average of the spectra of the Mg-MB and Ba-MB end members, as demonstrated in earlier studies [52,55] for various borate and silicate glasses. Despite the uncertainties of normalization, the variation in site environment of the barium ions is evident by the down shift of the respective cation motion band upon decreasing Ba content.

4. Property-structure correlations

The density of the lithium aluminoborate glasses is found to increase with the increase of the mass of the added alkaline earth cation, as expected for glasses with a higher molar mass. Also, the molar volume increases in the same direction, indicating that the structure becomes more open as the larger and heavier alkaline earth ions are incorporated into the glass (Table 1). The relative integrated intensity of the band envelopes arising from the asymmetric stretching of tetrahedral and trigonal borate groups are listed in Table 2. Lacking the exact absorption coefficients of BO₃ and BO₄ groups in the glasses of the current study, we make the approximation that they are equal and use the relative integrated intensities A_3 (800–1200 cm^{-1}) and A_4 (1200–1600 cm^{-1}) to estimate the fraction of boron atoms in four-fold coordination N_4 from $N_4 = A_4/(A_4 + A_3)$. As can be seen from Table 2, the estimated N_4 fraction decreases from Ba \approx Sr > Ca > Mg. Also, the

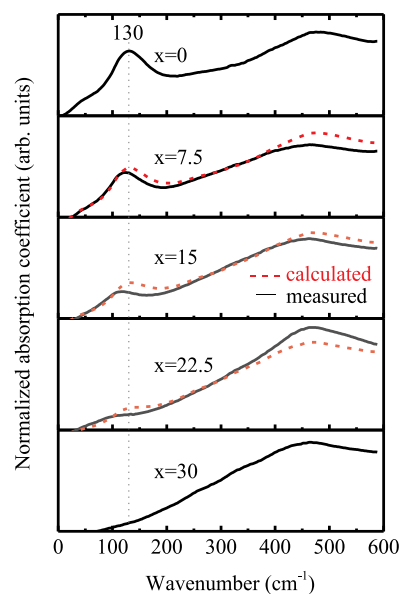


Fig. 9. Variations in the far-infrared spectra of the mixed alkaline-earth x MgO-(30-x) BaO-10Li₂O-10Al₂O₃-50B₂O₃ glass series. The solid black line shows the experimentally obtained IR spectra, the red broken line the calculated spectra using the weighted averages of the spectra of the Ba-MB and Mg-MB end members. (For interpretation of the references to color in this figure legend, the reader is referred to the web version of this article.)

N_4 value decreases with increasing MgO content in the mixed Mg/Ba-MB series (e.g. N_4 decreases with decreasing basicity of the glass). The N_4 values for single alkaline modified glasses of the present study were compared to other metaborate glasses [14,22] (see Table 2). Good agreement in the N_4 behavior could be noticed, with the slightly higher values for our glasses may be due to the presence of Al or Li.

Variations of the glass transition temperature T_g with the N_4 fraction, which expresses the cross-linking of the borate network by B-O-B bonds, and with the force constant $F_{\text{M-O}}$ which presents the strength of the cross-linking of the network by O-M-O bonds, are shown in Fig. 10a and 10b, respectively. The T_g of the prepared glass was determined from onset temperature (examples of DTA spectra are represented Fig. 11). When compared with other reported T_g values for binary alkaline borates such as 50B₂O₃-50MgO (646 °C), 50B₂O₃-50CaO (635 °C), 53B₂O₃-47SrO (603 °C) and 50B₂O₃-50BaO (559 °C) [4,21], the prepared single alkaline oxide modified lithium aluminoborate glass is found to be of lower T_g , perhaps due to the combined effect of network overmodification, since Al₂O₃ adds extra oxygen compared to the metacomposition and a lowering of the average cross-linking strengths of the cations, the high field strength Al₃₊ ions not compensating for the weaker cross linker Li+. As shown earlier for alkaline earth and transition metal metaborate glasses [4,22], a strong cross-linking capability of the modifier cations manifested by $F_{\text{M-O}}$ has a stronger influence on T_g than the degree of borate polymerization manifested by N_4 . Apparently, this is true also for the aluminoborate glasses of the current study, for which the high field strength ion Mg²⁺ leads to the highest T_g , despite the fact that these glasses have the lowest N_4 value (Fig. 10a). Comparison of the two series allows further interpretation.

Fig. 12 shows an interesting correlation between the optical basicity Λ_{th} and the glass transition temperature T_g in the aluminoborate glasses of the current study, an apparent invert correlation between the optical basicity Λ_{th} and the glass transition temperature T_g is obtained for both series was obtained. As can be noticed, alkaline earth cations of low field strength, i.e. low polarization power, lead to higher Λ_{th} and lower T_g . The opposite effect is found for cations of high field strength, because of their strong polarizing power on the oxygen atoms forming their coordination sphere (low Λ_{th} and high T_g).

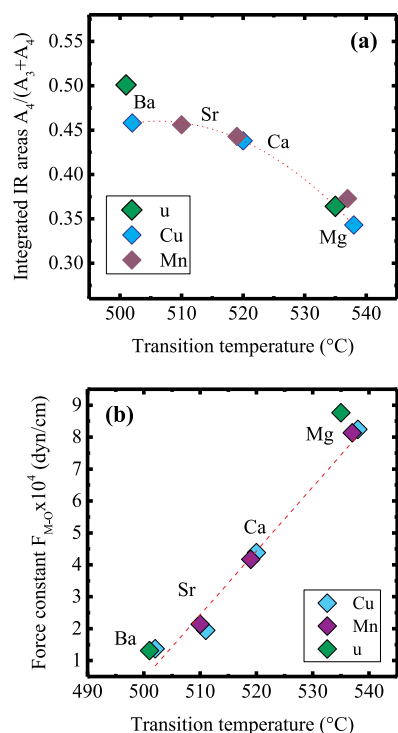


Fig. 10. Variation of the glass transition temperature T_g (with error $\pm 2^\circ\text{C}$) of the single alkaline earth 30MO-10Li₂O-10Al₂O₃-50B₂O₃ glasses (M = Ba, Sr, Ca and Mg) with (a) the N_4 fraction of the borate network, as derived from the integrated band intensities corresponding trigonal and tetrahedral borate units, and (b) the force constant F_{M-O} of M-O bonding, as derived from the far IR frequencies, $\nu(M-O)$.

5. Conclusions

Copper or manganese doped, as well as undoped glass samples, of the single alkaline-earth series 30MO-10Li₂O-10Al₂O₃-50B₂O₃ (M = Ba, Sr, Ca, Mg) and the mixed alkaline-earth series $x\text{MgO}-(30-x)\text{BaO}-10\text{Li}_2\text{O}-10\text{Al}_2\text{O}_3-50\text{B}_2\text{O}_3$ were prepared by melt quenching. Similar samples with and without dopants showed a good reproducibility of their properties, such as density, molar volume, refractive index and transition temperature T_g . The molar volume increases with increasing mass of the alkaline earth cation, indicating that the structures become more open. Infrared and Raman spectroscopies were employed to study structural variations between the

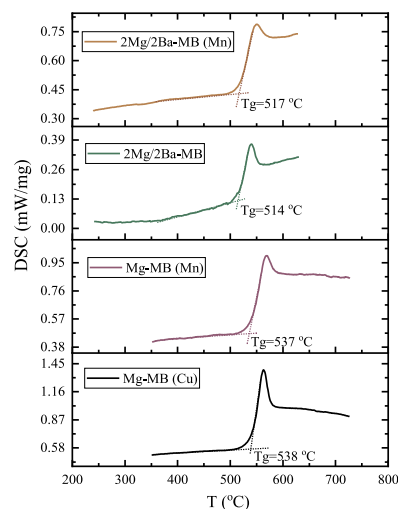


Fig. 11. An example of the glass transition temperature T_g (with error $\pm 2^\circ\text{C}$) of the prepared glasses

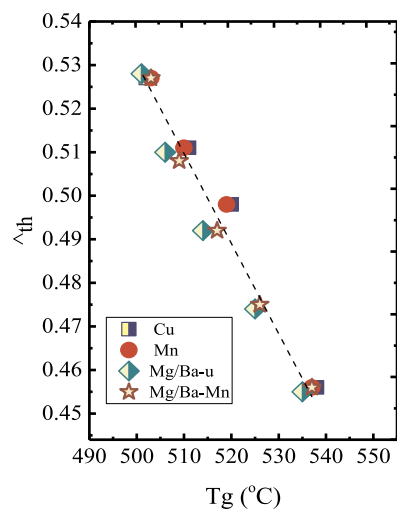


Fig. 12. Change of T_g with basicity of the prepared glasses. The first two “Cu” and “Mn” are the 30MO glasses while the 3rd and 4th are the mixed $x\text{MgO}-(30-x)\text{BaO}-10\text{Li}_2\text{O}-10\text{Al}_2\text{O}_3-50\text{B}_2\text{O}_3$ borate series undoped and Mn doped glasses.

glasses. The fraction of four-coordinated boron atoms N_4 was estimated from the integrated infrared intensities of absorption bands attributed to tetrahedral BO_4 and trigonal BO_3 borate units in the mid-infrared range. It was found that N_4 decreases in the order $\text{Ba} \approx \text{Sr} > \text{Ca} > \text{Mg}$, in agreement with the results from Raman spectroscopy. Mg-containing glasses showed not only a higher relative population of trigonal borate units than all other glasses, but also significant disproportionation of metaborate units into neutral BO_3 triangle and the highly charged pyroborate $\text{B}_2\text{O}_5^{4-}$ entities. The far-infrared spectra allow studying directly the site environment of the alkaline earth modifier cations. The frequency of cation-oxygen vibrations $\nu(M-O)$ shifts to lower values with increasing cation mass. For the mixed Mg/Ba-MB glass series, the Ba^{2+} cation motion band is shifted further to lower frequencies into the far-IR, the more Mg-ions are present in the glass. The high-field strength Mg^{2+} ions seek out favorable bonding sites with high negative charge, leaving the low energy sites for Ba^{2+} ions. This finding shows that dissimilar alkaline earth cations influence one another's atomic environment by polarization effects. Therefore the bonding and vibrational properties of metal ions are affected by the mixing of dissimilar cations, with the M-O interactions becoming stronger for the higher-field strength cation (Mg^{2+}) and weaker for the lower-field strength cation (Ba^{2+}). The force constant F_{M-O} for the M-O bonding was calculated from the far-IR frequencies and correlates favorable with the increase in glass transition temperature in the order $\text{Ba} < \text{Sr} < \text{Ca} < \text{Mg}$, this overriding the effect of a more depolymerized borate glass network in the same order, i.e. with decreasing N_4 . The theoretical optical basicity of the glasses as determined from glass composition, using the increment system of the glass constituent oxides, agrees well with the values obtained from the experimental oxygen polarizabilities as determined from the refractive index and density values. Only when using Mn^{2+} as the probe ion, the obtained basicity was found to be consistently higher than the theoretical optical basicity, indicating that Mn^{2+} ions seek out higher than the average basicity bonding sites.

CRedit authorship contribution statement

Hosam Othman: Conceptualization, Resources, Investigation, Formal analysis, Writing - review & editing, Supervision. **Hagar Elkholy:** Investigation, Visualization, Formal analysis, Writing - original draft. **Maria Rita Cicconi:** Investigation, Writing - review & editing. **Dimitrios Palles:** Investigation. **Dominique de Ligny:** Resources, Supervision, Writing - review & editing. **Efstratios I. Kamitsos:** Resources, Formal analysis, Writing - review & editing. **Doris Möncke:** Conceptualization, Writing - review & editing,

Visualization, Supervision, Formal analysis, Project administration, Validation.

Declaration of Competing Interest

The authors declare that they have no known competing financial interests or personal relationships that could have appeared to influence the work reported in this paper.

Acknowledgments

E.I. Kamitsos and D. Palles acknowledge support of the TPCI-NHRF work by the NSRF 2014-2020 Operational Program (grant number MIS 5002409) co-financed by Greece and the European Union.

References

- [1] E. Kamitsos, A. Patsis, M. Karakassides, G. Chryssikos, Infrared reflectance spectra of lithium borate glasses, *J. Non Cryst. Solids* 126 (1990) 52–67, [https://doi.org/10.1016/0022-3093\(90\)91023-k](https://doi.org/10.1016/0022-3093(90)91023-k).
- [2] E. Kamitsos, G. Chryssikos, Borate glass structure by Raman and infrared spectroscopies, *J. Mol. Struct.* 247 (1991) 1–16, [https://doi.org/10.1016/0022-2860\(91\)87058-p](https://doi.org/10.1016/0022-2860(91)87058-p).
- [3] D. Ehr, Structure, properties and applications of borate glasses, *Glass Technol.* 41 (2000) 182–185.
- [4] Y.D. Yiannopoulos, G.D. Chryssikos, E.I. Kamitsos, Structure and properties of alkaline earth borate glasses, *Phys. Chem. Glasses* 42 (2001) 164–172.
- [5] A. Winterstein-Beckmann, D. Möncke, D. Palles, E. Kamitsos, L. Wondraczek, Structure–property correlations in highly modified Sr, Mn-borate glasses, *J. Non Cryst. Solids* 376 (2013) 165–174, <https://doi.org/10.1016/j.jnoncrysol.2013.05.029>.
- [6] A. Winterstein-Beckmann, D. Möncke, D. Palles, E.I. Kamitsos, L. Wondraczek, Structure and Properties of Orthoborate Glasses in the $\text{Eu}_2\text{O}_3\text{-(Sr,Eu)O-B}_2\text{O}_3$ Quaternary, *J. Phys. Chem. B* 119 (2015) 3259–3272.
- [7] D.S. Brauer, D. Möncke, Structure of bioactive silicate, phosphate and borate glasses, in: A.R. Boccaccini, D.S. Brauer, L. Hupa (Eds.), *Bioactive Glasses: Fundamentals, Technology and Applications*, Royal Society of Chemistry, 2016.
- [8] H.A. Othman, H.S. Elkholy, I.Z. Hager, Spectroscopic investigation of samarium-doped lead oxyfluoroborate glasses using photo and cathode luminescence, *Int. J. Appl. Glass Sci.* 8 (2016) 313–321, <https://doi.org/10.1111/ijag.12259>.
- [9] D. Möncke, M. Papageorgiou, A. Winterstein-Beckmann, N. Zacharias, Roman glasses coloured by dissolved transition metal ions: redox-reactions, optical spectroscopy and ligand field theory, *J. Archaeol. Sci.* 46 (2014) 23–36, <https://doi.org/10.1016/j.jas.2014.03.007>.
- [10] Z. Yao, D. Möncke, E. Kamitsos, P. Houzot, F. Célarié, T. Rouxel, et al., Structure and mechanical properties of copper–lead and copper–zinc borate glasses, *J. Non Cryst. Solids* 435 (2016) 55–68, <https://doi.org/10.1016/j.jnoncrysol.2015.12.005>.
- [11] D. Ehr, Zinc and manganese borate glasses - phase separation, crystallisation, photoluminescence and structure, *Eur. J. Glass Sci. Technol. Part B Phys. Chem. Glasses* 54 (2) (2013) 65–75.
- [12] I. Konidakis, C.-P.E. Varsamis, E.I. Kamitsos, D. Möncke, D. Ehr, Structure and properties of mixed Strontium – Manganese Metaphosphate glasses, *J. Phys. Chem. C* 114 (2010) 9125–9138, <https://doi.org/10.1021/jp101750t>.
- [13] D. Möncke, E.I. Kamitsos, A. Herrmann, D. Ehr, M. Friedrich, Bonding and ion–ion interactions of Mn²⁺ ions in fluoride-phosphate and boro-silicate glasses probed by EPR and fluorescence spectroscopy, *J. Non Cryst. Solids* 357 (2011) 2542–2551, <https://doi.org/10.1016/j.jnoncrysol.2011.02.017>.
- [14] H.A. Othman, A. Herrmann, D. Möncke, Mixed barium-lead borate glasses studied by optical and vibrational spectroscopy, *Int. J. Appl. Glass Sci.* 10 (2019) 339–348, <https://doi.org/10.1111/ijag.13100>.
- [15] J.A. Duffy, M.D. Ingram, S. Fong, Effect of basicity on chemical bonding of metal ions in glass and its relevance to their stability, *PCCP* 2 (2000) 1829–1833, <https://doi.org/10.1039/b000489h>.
- [16] J.A. Duffy, A review of optical basicity and its applications to oxidic systems, *Geochim. Cosmochim. Acta* 57 (1993) 3961–3970, [https://doi.org/10.1016/0016-7037\(93\)90346-x](https://doi.org/10.1016/0016-7037(93)90346-x).
- [17] W. Vogel, *Glass Chemistry*, (1994). doi:10.1007/978-3-642-78723-2.
- [18] A.C. Wright, Borate structures: crystalline and vitreous, *Phys. Chem. Glasses Eur. J. Glass Sci. Technol. Part B* 51 (2010) 1–39.
- [19] H. Doweidar, Consideration of the boron oxide anomaly, *J. Mater. Sci.* 25 (1990) 253–258, <https://doi.org/10.1007/bf00544216>.
- [20] E.I. Kamitsos, Infrared studies of borate glasses, *Phys. Chem. Glasses Eur. J. Glass Sci. Technol. Part B* (2003) 79–87.
- [21] N.P. Lower, J.L. Mcrae, H.A. Feller, A.R. Betzen, S. Kapoor, M. Affatigato, et al., Physical properties of alkaline-earth and alkali borate glasses prepared over an extended range of compositions, *J. Non Cryst. Solids* 293–295 (2001) 669–675, [https://doi.org/10.1016/s0022-3093\(01\)00768-2](https://doi.org/10.1016/s0022-3093(01)00768-2).
- [22] D. Möncke, E.I. Kamitsos, D. Palles, R. Limbach, A. Winterstein-Beckmann, T. Honma, et al., Transition and post-transition metal ions in borate glasses: borate ligand speciation, cluster formation, and their effect on glass transition and mechanical properties, *J. Chem. Phys.* 145 (2016) 124501, <https://doi.org/10.1063/1.4962323>.
- [23] S. Feller, W. Dell, P. Bray, 10B NMR studies of lithium borate glasses, *J. Non Cryst. Solids* 51 (1982) 21–30, [https://doi.org/10.1016/0022-3093\(82\)90186-7](https://doi.org/10.1016/0022-3093(82)90186-7).
- [24] Y. Ohta, M. Shimada, M. Koizumi, Properties and Structure of Lithium Borate and Strontium Borate Glasses, *J. Am. Ceram. Soc.* 65 (1982) 572–574, <https://doi.org/10.1111/j.1151-2916.1982.tb10784.x>.
- [25] I. Konidakis, C. Varsamis, E. Kamitsos, Effect of synthesis method on the structure and properties of AgPO_3 -based glasses, *J. Non Cryst. Solids* 357 (2011) 2684–2689, <https://doi.org/10.1016/j.jnoncrysol.2011.03.013>.
- [26] N. Tagiara, D. Palles, E. Simandiras, V. Psycharis, A. Kyritsis, E. Kamitsos, Synthesis, thermal and structural properties of pure TeO_2 glass and zinc-tellurite glasses, *J. Non Cryst. Solids* 457 (2017) 116–125, <https://doi.org/10.1016/j.jnoncrysol.2016.11.033>.
- [27] E.I. Kamitsos, *Infrared Spectroscopy of Glasses*, in: M. Affatigato (Ed.), *Modern Glass Characterization*, John Wiley & Sons, Inc., 2015, pp. 32–73.
- [28] J.A. Duffy, Optical basicity of fluorides and mixed oxide–fluoride glasses and melts, *Phys. Chem. Glasses Eur. J. Glass Sci. Technol. Part B* 52 (2011) 107–114.
- [29] V. Dimitrov, T. Komatsu, An interaction of optical properties of oxidized oxide glasses in term of the electronic ion polarizability and average single bond strength (REVIEW), *J. Univ. Chem. Technol. Metall.* 45 (2010) 219–250.
- [30] V. Dimitrov, S. Sakka, Electronic oxide polarizability and optical basicity of simple oxides. I, *J. Appl. Phys.* 79 (1996) 1736–1740, <https://doi.org/10.1063/1.360962>.
- [31] J.A. Duffy, *Bonding, Energy Levels, and Bands in Inorganic Solids*, Longman Scientific and Technical, 1990.
- [32] J.A. Duffy, Optical basicity: a practical acid-base theory for oxides and oxyanions, *J. Chem. Educ.* 73 (1996) 1138, <https://doi.org/10.1021/ed073p1138>.
- [33] J.A. Duffy, B. Harris, E.I. Kamitsos, G.D. Chryssikos, Y.D. Yiannopoulos, Basicity variation in network oxides: distribution of metal ion sites in borate glass systems, *J. Phys. Chem. B* 101 (1997) 4188–4192, <https://doi.org/10.1021/jp9637542>.
- [34] C.P. Rodriguez, J.S. McCloy, M.J. Schweiger, J.V. Crum, A.E. Wanschell, Optical Basicity and Nepheline Crystallization in High Alumina Glasses, (Report PNNL-20184; EMSP-RPT-003), Pacific Northwest National Lab, (PNNL Richland, WA United States), 2011, <https://doi.org/10.2172/1019213>.
- [35] J.A. Duffy, The importance of π -bonding in glass chemistry: borate glasses, *Phys. Chem. Glasses Eur. J. Glass Sci. Technol. Part B* 49 (2008) 317–325.
- [36] N. Ohtori, M. Togashi, K. Takase, K. Handa, J. Ide, E.I. Kamitsos, K. Itoh, T. Fukunaga, N. Umesaki, MD study of sodium borate glasses containing Al_2O_3 , *Phys. Chem. Glasses Eur. J. Glass Sci. Technol. Part B* 47 (2006) 323–327.
- [37] E. Kamitsos, Y. Yiannopoulos, C. Varsamis, H. Jain, Structure-property correlation in glasses by infrared reflectance spectroscopy, *J. Non Cryst. Solids* 222 (1997) 59–68, [https://doi.org/10.1016/s0022-3093\(97\)90097-1](https://doi.org/10.1016/s0022-3093(97)90097-1).
- [38] E. Kordes, Physikalisch-chemische Untersuchungen über den Feinbau von Gläsern. I. Mitteilung. Die Molrefraktion binärer Phosphat-, Silikat- und Boratgläser, *Z. Für Anorg. Und Allg. Chem.* 241 (1939) 1–38, <https://doi.org/10.1002/zaac.19392410101>.
- [39] E. Kordes, Die Ermittlung von Atomabständen aus der Lichtbrechung, *Z. für Phys. Chem.* 44 (1) (1939) 249–260.
- [40] V. Dimitrov, T. Komatsu, Optical basicity and chemical bonding of Bi_2O_3 containing glasses, *J. Non Cryst. Solids* 382 (2013) 18–23, <https://doi.org/10.1016/j.jnoncrysol.2013.10.005>.
- [41] J.A. Duffy, E.I. Kamitsos, G.D. Chryssikos, A.P. Patsis, Trends in local optical basicity in sodium-borate glasses and relation to ionic mobility, *Phys. Chem. Glasses* 34 (1993) 153–157.
- [42] E. Kamitsos, G. Chryssikos, A. Patsis, J. Duffy, Metal ion sites in oxide glasses relation to glass basicity and ion transport, *J. Non Cryst. Solids* 196 (1996) 249–254, [https://doi.org/10.1016/0022-3093\(95\)00595-1](https://doi.org/10.1016/0022-3093(95)00595-1).
- [43] D. Möncke, H. Bradtmüller, G. Souza, M. Rodrigues Alisson, H. Elkholy, H. Othman, B. Moulton, E. Kamitsos, A. Rodrigues, D. Ehr, M. da Cruz Barbosa Neto, $\text{NaPO}_3\text{-AlF}_3$ glasses: fluorine evaporation during melting and the resulting variations in structure and properties, *J. Chem. Technol. Metall.* 53 (2018) 1047–1060.
- [44] L.L. Velli, C.P.E. Varsamis, E.I. Kamitsos, D. Möncke, D. Ehr, Optical basicity and refractivity in mixed oxyfluoride glasses, *Phys. Chem. Glasses Eur. J. Glass Sci. Technol. Part B* 49 (2008) 182–187.
- [45] W.L. Konijnendijk, The structure of borosilicate glasses, *Philips Res. Rep. Suppl.* 1 (1975) 1–243.
- [46] E.I. Kamitsos, M.A. Karakassides, G.D. Chryssikos, Vibrational spectra of magnesium-sodium-borate glasses. 2. Raman and mid-infrared investigation of the network structure, *J. Phys. Chem.* 91 (1987) 1073–1079, <https://doi.org/10.1021/j100289a014>.
- [47] E.I. Kamitsos, M.A. Karakassides, G.D. Chryssikos, Cation-network interactions in binary alkali metal borate glasses. A far-infrared study, *J. Phys. Chem.* 91 (1987) 5807–5813, <https://doi.org/10.1021/j100306a058>.
- [48] B. Meera, A. Sood, N. Chandrabhas, J. Ramakrishna, Raman study of lead borate glasses, *J. Non Cryst. Solids* 126 (1990) 224–230, [https://doi.org/10.1016/0022-3093\(90\)90823-5](https://doi.org/10.1016/0022-3093(90)90823-5).
- [49] G. Chryssikos, J. Kapoutsis, A. Patsis, E. Kamitsos, A classification of metaborate crystals based on Raman spectroscopy, *Spectrochim. Acta Part A Mol. Spectrosc.* 47 (1991) 1117–1126, [https://doi.org/10.1016/0584-8539\(91\)80043-i](https://doi.org/10.1016/0584-8539(91)80043-i).
- [50] S. Krishnaswami, H. Jain, E. Kamitsos, J. Kapoutsis, Connection between the microwave and far infrared conductivity of oxide glasses, *J. Non Cryst. Solids* 274 (2000) 307–312, [https://doi.org/10.1016/s0022-3093\(00\)00193-9](https://doi.org/10.1016/s0022-3093(00)00193-9).
- [51] E. Kamitsos, M. Karakassides, A. Patsis, G. Chryssikos, Laser-induced crystallization of glassy caesium metaborate studied by Raman spectroscopy, *J. Non Cryst. Solids* 116 (1990) 115–122, [https://doi.org/10.1016/0022-3093\(90\)91053-t](https://doi.org/10.1016/0022-3093(90)91053-t).
- [52] L.G. Bäck, S. Ali, S. Karlsson, D. Möncke, E.I. Kamitsos, B. Jonson, Mixed alkali/

- alkaline earth-silicate glasses: physical properties and structure by vibrational spectroscopy, *Int. J. Appl. Glass Sci.* 10 (2019) 349–362, <https://doi.org/10.1111/ijag.13101>.
- [53] L.L. Velli, C.P.E. Varsamis, E.I. Kamitsos, D. Möncke, D. Ehrhart, Structural investigation of metaphosphate glasses, *Phys. Chem. Glasses* 46 (2005) 178–181.
- [54] E.I. Kamitsos, W.M. Risen, Vibrational spectra of single and mixed alkali pentasilicate glasses, *J. Non Cryst. Solids* 65 (1984) 333–354, [https://doi.org/10.1016/0022-3093\(84\)90057-7](https://doi.org/10.1016/0022-3093(84)90057-7).
- [55] E.I. Kamitsos, A.P. Patsis, G.D. Chryssikos, Interactions between cations and the network in mixed alkali borate glasses, *Phys. Chem. Glasses* 32 (1991) 219–221.
- [56] A. Vegiri, C.-P.E. Varsamis, E.I. Kamitsos, Molecular dynamics investigation of mixed-alkali borate glasses: Short-range order structure and alkali-ion environments, *Phys. Rev. B* (2009) 80, <https://doi.org/10.1103/physrevb.80.184202>.
- [57] K. Griebenow, U. Hoppe, D. Möncke, E.I. Kamitsos, L. Wondraczek, Transition-metal incorporation and Co-Sr/Mn-Sr mixed-modifier effect in metaphosphate glasses, *J. Non Cryst. Solids* 460 (2017) 136–145, <https://doi.org/10.1016/j.jnoncrysol.2017.01.022>.
- [58] K. Griebenow, E.I. Kamitsos, L. Wondraczek, Mixed-modifier effect in (Ca,Mg) metaphosphate glasses, *J. Non Cryst. Solids* 468 (2017) 74–81, <https://doi.org/10.1016/j.jnoncrysol.2017.04.036>.
- [59] K. Griebenow, C.B. Bragatto, E.I. Kamitsos, L. Wondraczek, Mixed-modifier effect in alkaline earth metaphosphate glasses, *J. Non Cryst. Solids* 481 (2018) 447–456, <https://doi.org/10.1016/j.jnoncrysol.2017.11.041>.